JOURNAL OF MAGNETIC RESONANCE **129,** 134–144 (1997)
ARTICLE NO. MN971268

Technique for Importing Greater Evolution Resolution in Multidimensional NMR Spectrum

Gary McGeorge, Jian Zhi Hu, Charles L. Mayne, D. W. Alderman, Ronald J. Pugmire, and David M. Grant[1]

Department of Chemistry, University of Utah, Salt Lake City, Utah 84112

Received July 9, 1997

A very simple and general procedure that extracts constant-evolution-frequency data from a truncated multidimensional (2D, 3D, 4D, etc.) FID is described, generalized, analyzed, and illustrated. The method replaces Fourier transformation of the evolution dimension with a linear model created from a separate, high-quality 1D FID. The equivalent of high resolution in the evolution dimension can be achieved without obtaining an extensive multidimensional FID. The analysis of the 1D FID can also be used to predict the signal to noise ratio of the extracted slices that will result from various evolution dimension sampling protocols, making it possible to develop *a priori* an optimal sampling strategy for the multidimensional FID. The evolution dimension need not be sampled periodically. The procedure has a potential signal-to-noise ratio advantage because it extracts usable information from a multidimensional FID at short evolution times before the magnetization has decayed significantly.

INTRODUCTION

Although multidimensional NMR spectroscopy is remarkably powerful, its application often suffers from the lengthy experimental times required to acquire sufficient resolution in indirectly detected evolution dimensions. This limitation may be especially frustrating in those cases where an equivalent, well-resolved spectrum may be obtained relatively quickly from a 1D direct-detection experiment. For example, in solid state NMR the slow-sample-turning 2D PHORMAT experiment (*1, 2*) displays an isotropic shift spectrum in the evolution dimension, whereas this same spectral information is readily available from a high-speed magic-angle-spinning (MAS) 1D experiment. Likewise, in the single-crystal 2D chemical shift correlation experiment (*3, 4*) the evolution dimension spectrum can be obtained directly by taking a 1D spectrum with the crystal in its evolution position. In both cases it is much easier to obtain high resolution by fully sampling the 1D free induction decay (FID) than by extending the 2D FID to long evolution times.

Manassen *et al.* (*5*) first proposed in 1987 that information from 1D spectra could be transferred into the analysis of 2D data with linear least-squares procedures. In the meantime much attention has been focused on linear prediction (*6*) and maximum entropy (*7*) as a means of increasing resolution in evolution dimensions, and the usefulness of the simple least-squares alternative has not been appreciated. This paper re-examines, generalizes, and analyzes the linear least-squares procedure, and presents examples from solid state NMR that illustrate its power. It is shown that closely spaced constant-evolution-frequency slices can be extracted from a truncated multidimensional FID, here called the ''main'' FID, with the aid of data from a separate 1D FID, called the ''guide'' FID. The procedure may be thought of as exporting resolution from the guide FID, and importing it into the associated evolution dimension of the main FID. Thus our acronym, ''TIGER,'' is derived from technique for importing greater evolution resolution. TIGER can also be seen as a generalization of the 1D chemical shift modulated correlation spectroscopy (*8*) developed for single crystals.

TIGER is applicable to any multidimensional spectroscopy with an evolution dimension for which an equivalent high-resolution 1D FID can be obtained. It also requires that the main multidimensional FID be composed of sums of products of responses (see below). TIGER replaces Fourier transformation of the designated evolution dimension with a linear model created from the guide FID. Applying the linear model to the truncated experimental main FID then directly extracts constant-evolution-frequency slices equivalent to those that could be separated by Fourier transformation of a much-expanded evolution dimension FID. Thus, the equivalent of high resolution in the evolution dimension is achieved without obtaining an extensive main FID. TIGER accommodates any magnetization-decay function, as the character of the decay is observed directly in the corresponding 1D guide FID. TIGER is thus more general than linear prediction (*6*), which requires exponential magnetization decay. TIGER automatically incorporates the matched filter that optimizes the signal-to-noise ratio (S/N) when Fourier

[1] To whom correspondence should be addressed.

1090-7807/97 $25.00

transforming a FID; each peak receives its own matched filter according to its individual width. Since Fourier transformation is bypassed, the main evolution dimension need not be sampled periodically (5). Thus TIGER also provides a simple, alternative procedure for treating such data. The analysis of the guide FID also predicts the S/N of the extracted slices that will result from various evolution-dimension sampling protocols, making it possible to develop *a priori* an optimal sampling strategy for the main FID. When compared to Fourier transform processing of an evolution dimension, TIGER has a potential S/N advantage that arises from its ability to extract information from a multidimensional FID acquired at short times before the magnetization amplitude has decayed significantly.

THEORY

The linear least-squares procedure applies only to those multidimensional NMR experiments that produce main FIDs that can be written as a sum of products of responses in two complementary sets of dimensions. For example, in the 2D case the main FID must be a sum of products of responses in the acquisition dimension and the evolution dimension. Each such product typically corresponds to a unique nuclear site in a molecule. The application of the linear model is different for phase-encoded complex and amplitude-modulated hypercomplex main FIDs (*9, 10*). The original work (*5*) applied to complex 2D FIDs, and this case is treated first.

Complex phase-encoded main FIDs. For M nuclear sites indexed by m, the noiseless 2D main FID must be written in the sum-of-products functional form

$$F(t_b, t_a) = \sum_{m=1}^{M} g_m(t_b) f_m(t_a), \qquad [1]$$

where t_b is the evolution time and t_a parameterizes the acquisition dimension. The standard complex notation is adopted for $F(t_b, t_a)$, $g_m(t_b)$ and $f_m(t_a)$. The acquisition dimension quadrature-detected responses $f_m(t_a)$ that constitute the 2D FID are each phase shifted to encode their evolution frequencies by multiplication with the complex function $g_m(t_b)$. The $g_m(t_b)$ functions give the evolution response from the mth site, while the $f_m(t_a)$ functions are the corresponding acquisition dimension responses. It is the individual $f_m(t_a)$ functions, separated from one another by the information gathered in the evolution dimension, that are sought from the 2D data. By sampling at N evolution times denoted by τ_n, a set of N linear equations valid at all t_a is produced

$$F(\tau_n, t_a) = \sum_{m=1}^{M} g_m(\tau_n) f_m(t_a), \qquad [2]$$

where $F(\tau_n, t_a)$ is the 2D FID sampled at τ_n in the evolution dimension, and the $g_m(\tau_n)$ are sampled $g_m(t_b)$ functions.

The central idea of the original work (*5*) and of this paper is that the values of the $g_m(\tau_n)$ are available from the decomposition of the 1D guide FID into contributions from each individual site. The process of analyzing the guide spectrum is not trivial, but it can be accomplished by simulating and fitting the 1D guide FID whenever its spectrum is at least partially resolved (see below).

Once the $g_m(\tau_n)$ coefficients have been obtained from the 1D guide FID, the process of extracting the $f_m(t_a)$ from the main FID follows from the linear model (*11, 12*). Thus, when $M \leq N$, least-squares estimates $\hat{f}_m(t_a)$ for the acquisition dimension responses are found from the equations

$$\hat{f}_m(t_a) = \sum_{n=1}^{N} h_{m,n} E(\tau_n, t_a), \qquad [3]$$

where $E(\tau_n, t_a)$ gives the sampled experimental 2D FID that includes noise. The $h_{m,n}$ coefficients are found from

$$h_{m,n} = \sum_{m'=1}^{M} b_{m,m'} g^*_{m'}(\tau_n), \qquad [4]$$

where the $b_{m,m'}$ are the solutions to

$$\delta_{m,m'} = \sum_{m''=1}^{M} b_{m,m''} \sum_{n=1}^{N} g^*_{m''}(\tau_n) g_{m'}(\tau_n), \qquad [5]$$

and where $\delta_{m,m'}$ is the Kronecker delta. The complex nature of the $g_m(\tau_n)$ introduces the complex conjugate into Eqs. [4] and [5]. Equations [3], [4], and [5] describe a very simple and fast computation consisting only of matrix multiplications and inversion of the positive definite $M \times M$ square matrix with elements $\Sigma_{n=1}^{N} g^*_m(\tau_n) g_{m'}(\tau_n)$. The above procedure is the standard linear model (*11, 12*), often written in matrix notation as

$$\hat{\mathbf{f}}(t_a) = \mathrm{BG}\dagger\mathbf{E}(t_a) = (\mathrm{G}\dagger\mathrm{G})^{-1}\mathrm{G}\dagger\mathbf{E}(t_a).$$

For phase-encoded complex data the linear model extracts the acquisition responses $\hat{f}_m(t_a)$ directly without Fourier transformation, hence phase-twisted 2D peaks are not encountered. The extracted responses $\hat{f}_m(t_a)$ are acquisition dimension FIDs that can be Fourier transformed and phased to absorption mode lineshapes. This feature alone recommends the linear model for processing phase-encoded multidimensional NMR data.

Hypercomplex amplitude-modulated main FIDs. In hypercomplex amplitude-modulated data (*10*) separate real and imaginary designations are needed for each dimension (*9*). The acquisition-dimension quadrature-detected FIDs are

each amplitude modulated by cosine and sine functions of the corresponding evolution frequency. Those that are cosine-modulated are labeled real in the evolution dimension, and those that are sine-modulated are labeled imaginary. The amplitude modulating factors are thus real functions that exist in pairs that may be designated $g_{m,\rho}(\tau_n)$, where the additional subscript ρ denotes real or imaginary. In the context of the main 2D FID, ρ refers to real and imaginary in the evolution dimension, whereas in the context of the 1D guide FID, ρ refers to the acquisition-dimension quadrature-detection axes. The main FIDs real and imaginary parts must also be labeled with the same symbol ρ, becoming $F_\rho(\tau_n, t_a)$. Equation [2] then becomes the $2N$ linear equations valid for all t_a

$$F_\rho(\tau_n, t_a) = \sum_{m=1}^{M} g_{m,\rho}(\tau_n) f_m(t_a). \quad [6]$$

Equation [3] is modified to expand its sum to include the real and imaginary (in the evolution dimension) contributions

$$\hat{f}_m(t_a) = \sum_{\rho=\text{real}}^{\text{imag}} \sum_{n=1}^{N} h_{m,\rho,n} E_\rho(\tau_n, t_a), \quad [7]$$

Eq. [4] becomes

$$h_{m,\rho,n} = \sum_{m'=1}^{M} b_{m,m'} g_{m',\rho}(\tau_n), \quad [8]$$

and Eq. [5] becomes

$$\delta_{m,m'} = \sum_{m''=1}^{M} b_{m,m''} \sum_{\rho=\text{real}}^{\text{imag}} \sum_{n=1}^{N} g_{m'',\rho}(\tau_n) g_{m',\rho}(\tau_n). \quad [9]$$

As before, Eq. [9] defines an inverse relationship between two square matrices.

Analysis of the guide FID. For both the complex and hypercomplex cases, separation of the $\hat{f}_m(t_a)$ acquisition-dimension responses from the main FID is actually accomplished by decomposing the guide FID into the responses $g_m(\tau_n)$ and $g_{m,\rho}(\tau_n)$ respectively, and this step is the most crucial in the application of TIGER. For the examples given below, this decomposition is done by least-squares fitting the guide FID with a linear superposition of model FIDs adjusted in frequency and lineshape with a SIMPLEX algorithm until an overall best fit is obtained. The lineshape is modeled as a convolution of Lorentzian and Gaussian shapes, and thus the simulated response for each site is made to decay as the product of exponential and Gaussian functions in the traditional manner. The two decay constants and the frequency of the peak are varied with the SIMPLEX algorithm until a minimum sum of squares is obtained. The results of the fitting are the amplitudes, frequencies, lineshapes, and phases of the lines in the guide FID. The phase values obtained from the guide FID become irrelevant, as phase in the multidimensional FID is controlled by the main pulse sequence. The models are all scaled to $g_m(0) = 1$. This scaling has the effect of transferring the amplitude information in the main FID to the extracted responses, because of the sum-of-products form of Eqs. [1] and [6]. The frequencies and lineshapes from the fitting, along with phases determined by the main pulse sequence, then may be used to construct model FID functions $g_m(t)$ that, when appropriately sampled, provide the $g_m(\tau_n)$.

The guide FID may also be used to predict the optimal evolution-dimension sampling of the main FID. One would like to obtain, in a fixed period of time, a main FID that will produce extracted responses $\hat{f}_m(t_a)$ with the highest S/N. For periodic sampling, the variables to be optimized are the evolution dwell time and the maximum evolution time. In the nonperiodic sampling case, the goal is to find the set of evolution times τ_n (and in the hypercomplex case, the selection of real and imaginary FIDs) that will produce the highest S/N. Such optimization requires understanding the propagation of noise from the main FID into the responses $\hat{f}_m(t_a)$. Noise propagation in the linear model is characterized by the variance–covariance matrix given by $\sigma^2 b_{m,m'}$, where $b_{m,m'}$ is defined in Eq. [5] or Eq. [9] (*11*, *12*). The symbol σ denotes the variance of the data, equal to the rms noise level of the main FID. The matrix of correlation coefficients is given by

$$\rho_{m,m'} = b_{m,m'} (b_{m,m} b_{m',m'})^{-1/2}. \quad [10]$$

The marginal standard deviations σ_m are given by the square root of the diagonal terms of the variance–covariance matrix

$$\sigma_m = \sigma b_{m,m}^{1/2}, \quad [11]$$

and describe the rms noise level in the responses $\hat{f}_m(t_a)$ (*11*, *12*). If the main FID is gathered in a fixed period of time as N acquisition-dimension FIDs, the variance σ of the data in each 1D FID composing the main 2D FID will be proportional to $N^{-1/2}$, and the signal in each 1D FID is proportional to N^{-1}. Thus the S/N in each 1D FID will be proportional to $N^{-1/2}$, and the S/N of each extracted response $\hat{f}_m(t_a)$ is proportional to a figure of merit given by

$$s_m = (N b_{m,m})^{-1/2}. \quad [12]$$

Examples given below show how this figure of merit reflects some well-known properties of transient NMR signals. The figure of merit for a given peak depends not only on that peak's properties, but also on the frequencies and widths of

all the peaks in the spectrum and on the sampling protocol. The figure of merit as defined above gives the relative S/N for each peak as a function of the sampling protocol, but it does not specify the ratio of S/N between the various peaks. This is because the signal heights of the various peaks in the 2D spectrum depend upon the nature (e.g., the lineshape) of the acquisition dimension response in the main FID, and these characteristics cannot be determined from the guide FID alone.

With the convention that $g_m(0) = 1$, the maximum value that the figure of merit can attain is $s_m = 1$ for a single pulse applied to a sample with only one response. In the above analysis such an experiment is described by $M = 1$ and $N = 1$. The evolution time τ_n is effectively zero. Evaluating $b_{1,1}$ for this instance renders the figure of merit $s_1 = 1$.

The above derivation of the figure of merit addresses propagation of noise from the main FID to the extracted FIDs, but it ignores errors that originate in the guide FID and the fitting process that separates the $g_m(\tau_n)$ responses. Since the guide FID is 1D, its S/N is typically high and any such errors will be relatively small.

Differences between the guide FID and its separate models may be introduced both accidentally and intentionally. For example, the model may intentionally omit certain responses in order to forego modeling and extracting uninteresting or spurious peaks. Also, extra models that have no corresponding intensity in the main FID may be included. It will be shown below that such anomalies in the model do not impair the method when the extra or missing peaks are well separated from the other peaks, and thus it is often possible to omit uninteresting peaks without compromising the extraction of important peaks. Also, the method is not impaired if for some reason the guide FID includes an isolated response that does not appear in the main FID.

TIGER automatically incorporates the matched filter (*9*) into the processing of the evolution dimension. In the case of a single response whose evolution frequency is zero, the evolution response is given by $g_1^*(t_b) = d(t_b)$, where $d(t_b)$ is a real function characterizing the magnetization decay. Thus, from Eq. [4] with $M = 1$

$$h_{1,n} = b_{1,1} d(\tau_n), \qquad [13]$$

so that

$$\hat{f}_1(t_a) = b_{1,1} \sum_{n=1}^{N} d(\tau_n) E(\tau_n, t_a). \qquad [14]$$

Thus TIGER multiplies the main FID by the decay function determined from the guide FID, and this multiplication constitutes the application of a matched filter in the evolution dimension.

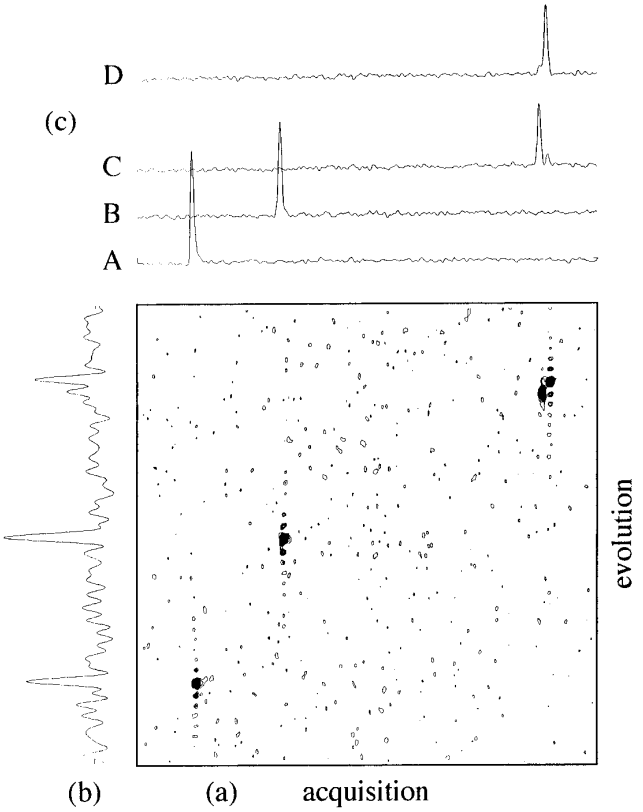

FIG. 1. Spectra obtained by Fourier transforming a 2D ^{13}C chemical-shift-correlation spectrum of succinic acid. (a) Two-dimensional spectrum, the hypercomplex Fourier transform of a FID with 45 evolution dwell increments. The complete spectral widths are plotted in both the acquisition and evolution dimensions. (b) Projection of the 2D spectrum onto the evolution axis. (c) Acquisition dimension slices corresponding to the four peaks. The spectral width in both dimensions is 1/66.7 μs = 14,992.5 Hz. There are 512 complex points in the acquisition dimension FIDs.

TIGER has a potential S/N advantage over Fourier transform processing of evolution dimensions. This advantage arises solely from TIGER's ability to obtain usable information from a short multidimensional FID acquired before the magnetization has decayed. If a multidimensional FID contains only a single response, treating the evolution dimension with TIGER is equivalent to processing it with a matched-filter and Fourier transform, and it will result in the same S/N. But when multiple peaks are present, Fourier transformation processing often requires an extensive FID that has decayed significantly in order to avoid interference between responses. The part of the experimental time spent sampling after the magnetization has decayed significantly in the evolution dimension is not used efficiently to gather acquisition-dimension-response information. TIGER can thus gain a S/N advantage by avoiding such long evolution times.

The above equations are derived under the assumption that the acquisition-dimension FIDs that constitute the main

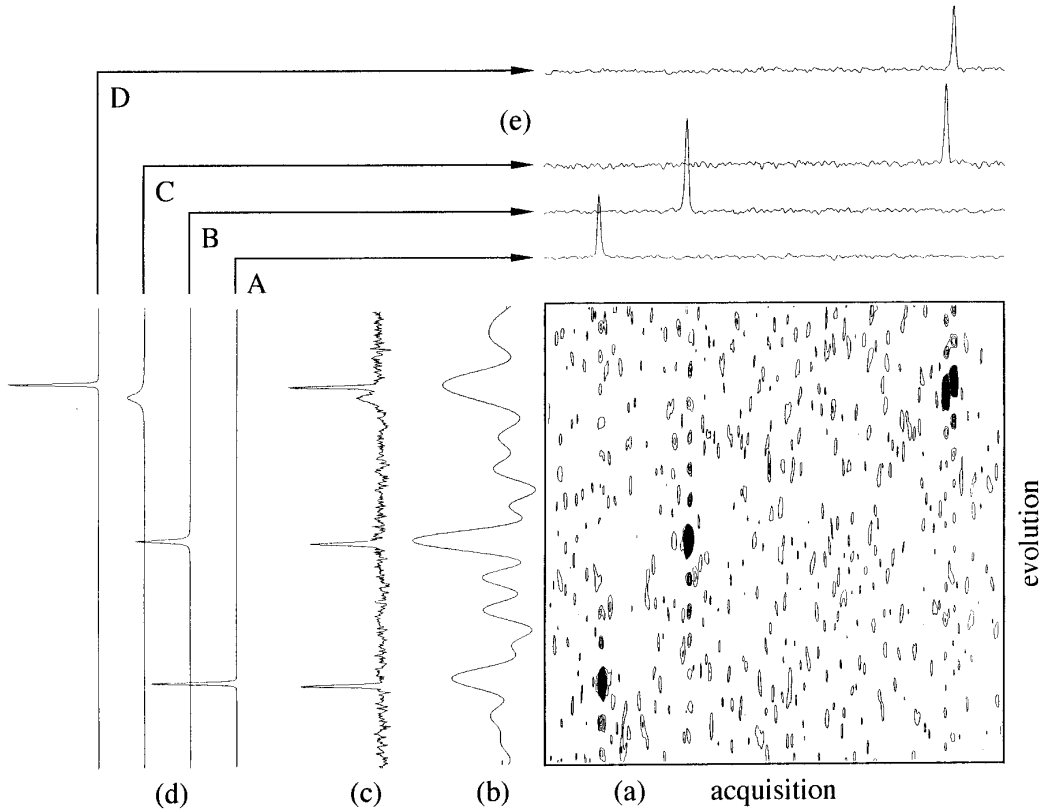

FIG. 2. Spectra obtained by TIGER processing a 2D ^{13}C chemical-shift-correlation spectrum of succinic acid. (a) Two-dimensional spectrum, the hypercomplex Fourier transform of the FID truncated to 15 complex evolution dwell increments. (b) Projection of the 2D spectrum onto the evolution axis. (c) Guide spectrum taken with the single crystal in the evolution orientation with 1024 complex points in its FID. (d) Simulated spectra that decompose the guide spectrum into four peaks. (e) Acquisition dimension spectra extracted from the main FID truncated to 15 evolution dwell increments, connected to their corresponding guide spectrum models with the labeled lines.

FID are all gathered with the same number of transients, and thus that they all have the same noise level. If selective signal averaging is used, it is appropriate to employ a weighted linear model. This extension is easily made by incorporating the variance–covariance matrix of the experimental data into Eqs. [4] and [5], or Eqs. [8] and [9]. Standard texts (*11, 12*) address these details.

TABLE 1
Parameters of Succinic Acid Peaks in Fig. 1[a]

Peak	Frequency[b]	Gaussian[c]	Lorentzian[c]
A	−0.315383	0.004760	0.000527
B	−0.005011	0.003666	0.004342
C	+0.304400	0.005617	0.017434
D	+0.333076	0.003973	0.001017

[a] These values produce the points in Fig. 4.

[b] Frequencies are given in a unit frequency scale that ranges from −0.5 on the left end to +0.5 at the right end of the spectrum.

[c] Broadenings are specified by their full-width at half-maximum on the unit frequency scale.

EXAMPLES

Chemical shift correlation spectroscopy. Single-crystal chemical shift correlation spectroscopy is a very simple 2D NMR experiment in which a single crystal is held stationary during the evolution period of a 2D chemical exchange pulse sequence, rotated during the mixing period, and then again held stationary in a second orientation during the acquisition period (*3, 4*). This protocol results in a 2D spectrum with peaks located at their chemical shifts in the two single-crystal orientations. This correlated shift information provides a means of measuring complete chemical-shift tensors in samples with many nonequivalent nuclei in their unit cells (*13, 14*). Figure 1 shows a ^{13}C chemical shift correlation spectrum of succinic acid obtained from Fourier transforming a hypercomplex FID with 45 evolution dwell increments, along with the projection onto the evolution axis and

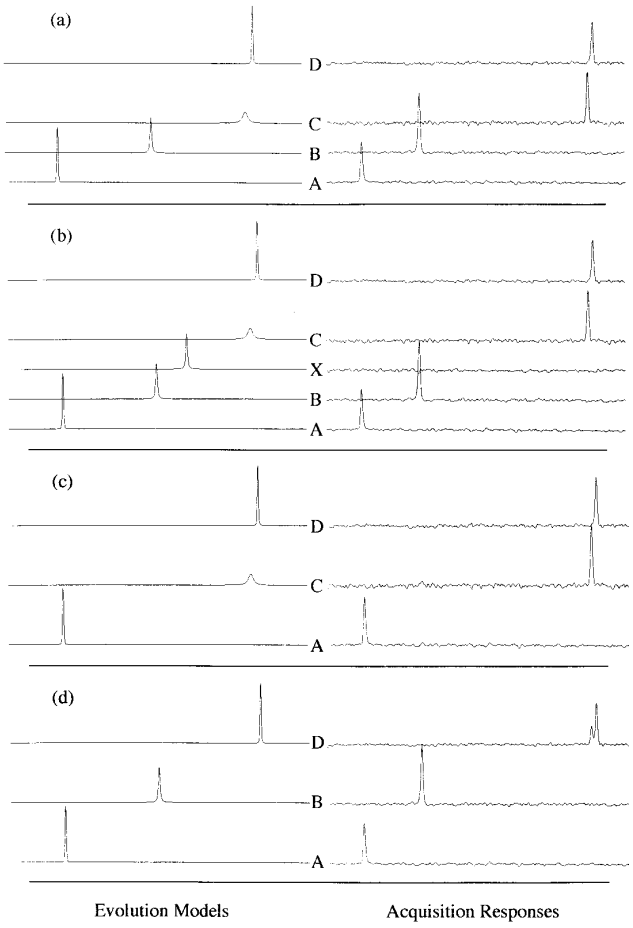

FIG. 3. Evolution dimension model sets and their corresponding acquisition dimension responses extracted from the succinic acid main FID of Fig. 2. (a) Same set of four simulated spectra A, B, C, and D used in Fig. 2. The extracted acquisition dimension responses are thus the same as in Fig. 2. (b) Set of four simulated spectra A, B, C, and D used in Fig. 1, plus a fifth model X that does not correspond to any feature in the guide FID or the main FID. The addition of the well-separated model X does not damage the extraction of the responses from the other four models, and its extracted response contains only noise. (c) Set of three simulated spectra A, C, and D, but not model B. The omission of the well-separated model B does not damage the extracted responses from the other three models. (d) Set of three simulated spectra A, B, and D, but not model C. The omission of the model C corrupts the extracted response from the nearby peak D.

acquisition dimension slices through the four peaks. No line broadening was applied to the evolution dimension, and peaks A, B, and D are narrow enough that $\sin(x)/x$ oscillations remain. Peak C is significantly broader in the evolution dimension due to difficulty in decoupling its CH_2 carbon at that particular single-crystal orientation. The slices for peaks C and D exhibit interference between the peaks due to the width of peak C and the $\sin(x)/x$ oscillations of peak D. Figure 2 shows the ^{13}C spectra associated with the TIGER analysis of the same main FID truncated to 15 evolution dwell increments, only 1/3 the actual data used for Fig. 1. The 2D spectrum obtained from the truncated 2D FID and the evolution-dimension-projection 1D spectrum both show large $\sin(x)/x$ oscillations, and peaks C and D are not resolved in the projection. The 1D guide spectrum, however, accurately characterizes both the frequencies and widths of all four peaks for this orientation of the crystal. The simulated spectra shown result from fitting the guide FID in the manner described above. The resulting frequency and broadening parameters for the guide spectrum in Fig. 2 are given in Table 1. The extracted responses shown at the top of Fig. 2 each contain only a single peak. All of the shift and correlation information available from the 2D spectrum is thus present in the extracted responses.

Figure 3 shows examples that illustrate the effects of omitting and including extra $g_m(\tau_n)$ models in the succinic acid case. Figure 3a serves as a point of reference, showing the same model set and extracted responses as in Fig. 2. In Fig. 3b an extra model X with an evolution dimension frequency that is well-separated from the other models has been included; the extracted responses for models A, B, C, and D remain unchanged, while the X response shows only noise. In Fig. 3c the response from the well-isolated peak B has been omitted from the set; the resulting extracted responses for peaks A, C, and D are not significantly changed. On the other hand, when the response from peak C is omitted from the set, as in Fig. 3d, the resulting extracted responses for the well-isolated peaks A and B are not significantly changed, but the extracted response for the nearby peak D is corrupted by the response that would otherwise have been assigned to peak C. Thus, to avoid such artifacts it is important that any omitted models be at well-separated evolution frequencies.

Figure 4 shows a plot of the S/N figures of merit s_n for periodic sampling of the succinic acid main FID as a function of the maximum evolution time, as specified by the number of evolution dwell increments. This plot illustrates a number of well-known properties of transient NMR signals. The acquisition-dimension responses from the narrow, isolated lines A and B always have relatively good S/N, even when only a few evolution dwell increments are sampled, as their magnetizations quickly separate from one another. On the other hand, when only a few evolution dwell increments are sampled the responses from the closely spaced lines C and D have very poor S/N because their magnetizations have not yet moved apart, making it difficult for the algorithm to separate the two signals. Plots (not shown) of the responses extracted from the main FID truncated to only 3 evolution dwell increments have very large noise amplitudes for lines C and D, and the noise in one of the extracted spectra is approximately the negative equal of the noise in the other, as predicted by the value of the correlation coefficient, $\rho_{C,D} = -0.977$. From the data

in Table 1 it can be calculated that the magnetizations of lines C and D precess to opposite phases in 17.4 evolution dwell times, and the plot in Fig. 4 shows that sampling the main FID out to this evolution time results in the responses of lines C and D having relatively good S/N. As the maximum evolution time is extended (under conditions of constant total experimental time) the S/N for peak C decreases because information is gathered less efficiently after its magnetization has decayed significantly. For the same reason the S/N for all of the lines ultimately fall as the maximum evolution time is increased. Fortunately, the plot of Fig. 4 shows a wide range of maximum evolution times, from 14 to 20 dwell increments, that give relatively good S/N for all four lines. Because the projection pulse that terminates the evolution period in the exchange pulse sequence leaves $\sqrt{1/2}$ of the magnetization on the average, the maximum possible figure of merit at large numbers of dwell increments is 0.707, and indeed all of the curves in Fig. 4 lie below this value. The irregularities in the figures of merit values for 3 through 8 dwell increments, particularly evident in the points for peak B, result whenever one of the limited number of dwell increments includes a particularly large or small projected magnetization. At larger numbers of dwell increments the curves become smoother as each additional FID makes a proportionately smaller contribution. The plot in Fig. 4 is based on the evolution dwell time that produces the spectral width shown in Fig. 2. Plots of the S/N figure of merit versus maximum evolution time are largely independent of the spectral width, except in those cases where aliasing causes overlap of lines.

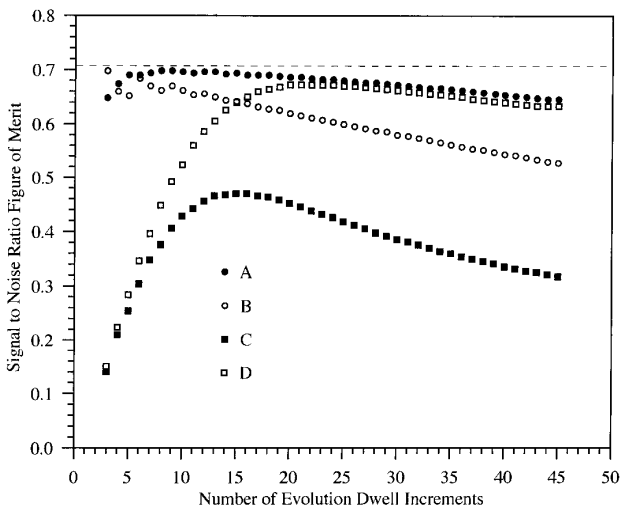

FIG. 4. Plot of the signal-to-noise figure of merit s_n for the four succinic acid peaks in Fig. 1 as a function of the number of dwell increments in the evolution dimension of the main FID. The number of dwell increments N includes the initial evolution time $t_b = 0$, so that the evolution times are given by $n\delta$, for $n = 0$ to $N - 1$. The dwell time is 66.7 μs, the same as that used for the spectrum of Fig. 1. The dashed line at 0.707 marks the maximum possible figure of merit for the 2D chemical-shift-correlation experiment.

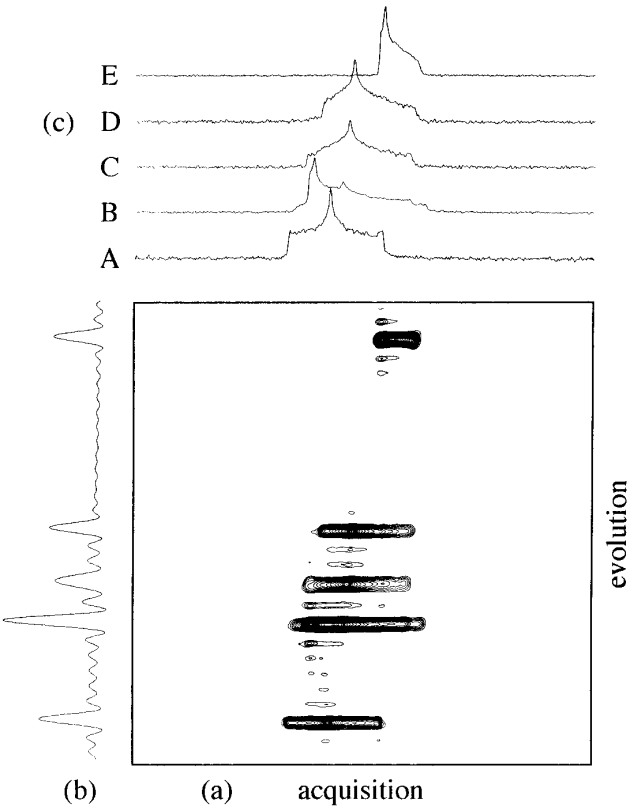

FIG. 5. Spectra obtained by Fourier transforming a 2D ^{13}C PHORMAT spectrum of 2,6-dimethoxynaphthalene. (a) Two-dimensional spectrum, the hypercomplex Fourier transform of a FID with 32 evolution dwell increments. The complete spectral widths are plotted in both the acquisition and evolution dimensions. (b) Projection of the 2D spectrum onto the evolution axis. (c) Acquisition dimension slices corresponding to the five peaks. The spectral width in the acquistion dimension is 80.0 kHz, and the spectral width in the evolution dimension is 12.5 kHz. There are 512 complex points in the acquisition dimension FIDs.

Magic angle turning spectroscopy. A number of 2D magic-angle-turning (MAT) experiments have recently been developed to obtain chemical shift powder patterns separated by their isotropic shifts in the evolution dimension (*1, 2, 15*). One variant is the phase-corrected MAT, or PHORMAT, experiment designed to produce nontilted spectra with flat baseplanes. Figure 5 shows a ^{13}C PHORMAT spectrum of 2,6-dimethoxynaphthalene, along with its evolution dimension projection and acquisition dimension slices. This spectrum was obtained from a hypercomplex FID with 32 evolution dwell increments, too few to suppress the $\sin(x)/x$ oscillations from the narrow peaks. Shown in Fig. 6 are the spectra associated with TIGER processing the main FID truncated to 8 evolution dwell

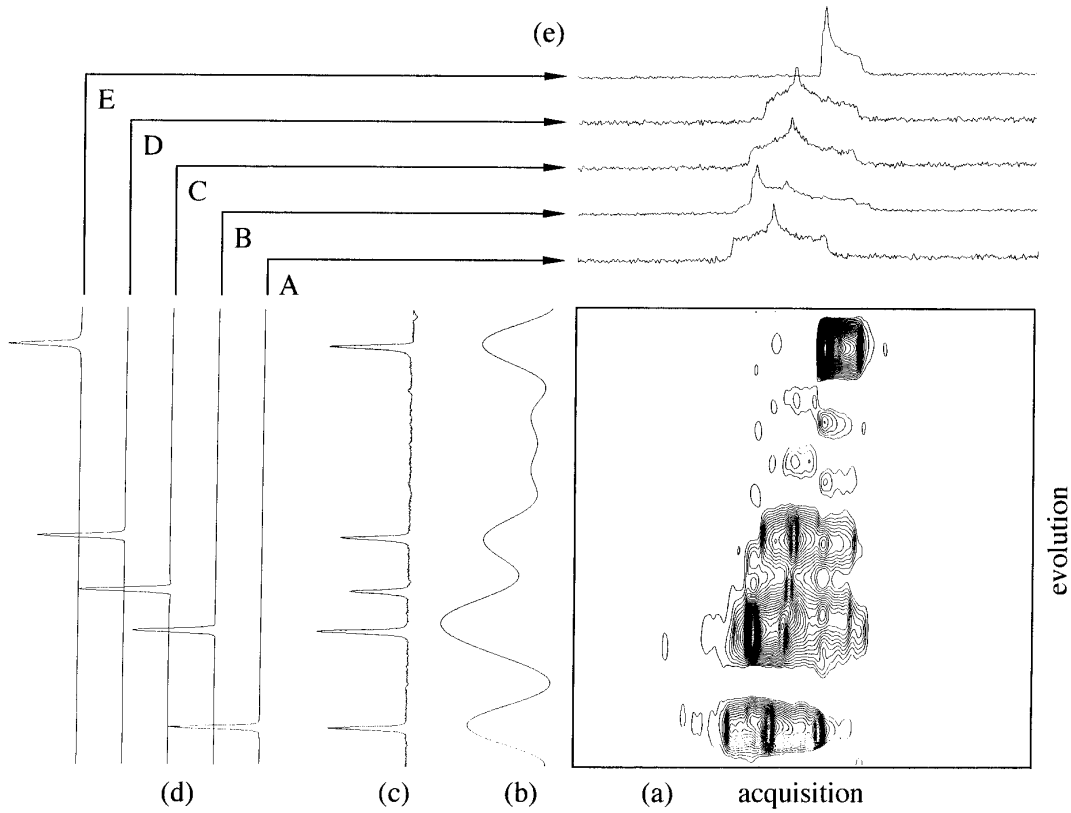

FIG. 6. Spectra obtained by TIGER processing a 2D ^{13}C PHORMAT spectrum of 2,6-dimethoxynaphthalene. (a) Two-dimensional spectrum, the hypercomplex Fourier transform of the FID used for Fig. 5 truncated to 8 evolution dwell increments. (b) Projection of the 2D spectrum onto the evolution axis. (c) High-speed MAS TOSS guide spectrum with 1024 complex points in its FID. (d) Simulated spectra that decompose the guide spectrum into five evolution dimension peaks. (e) Acquisition dimension spectra extracted from the main FID, connected to their corresponding guide spectrum models with the labeled lines.

increments, corresponding to only $\frac{1}{4}$ of the actual data used in Fig. 5. The guide spectrum was obtained by high-speed MAS using TOSS sideband suppression (*16*), and it was decomposed into the simulated spectra in the same manner as described above. Plotted at the top of Fig. 6 are the extracted powder patterns. Peak B represents two carbons with essentially identical isotropic shifts, but quite different principal values, and the breakpoints of both powder patterns may be seen in the extracted spectrum. It was impossible to distinguish the two different responses contained in peak B in the guide FID, and consequently their acquisition dimension responses are not separated by TIGER. Because the two tensors are so different, fitting the extracted spectrum with two powder patterns would provide the two sets of principal values (*17*).

TIGER processing significantly increases the power of the PHORMAT experiment, particularly when it is necessary to separate many peaks. Figure 7 shows results from TIGER processing a ^{13}C PHORMAT 2D FID obtained overnight on a 400-MHz spectrometer on caryophyllene oxide, a sesquiterpene with 15 carbons. The high-speed MAS 1D guide spectrum shown in Fig. 7a was obtained with TPPM decoupler modulation (*18*) and TOSS spinning-sideband suppression (*16*). The guide spectrum linewidths vary between 0.2 and 0.5 ppm. The closely spaced lines at 28.1 and 28.5 ppm are both approximately 0.3 ppm wide. The PHORMAT dataset, with a maximum evolution time of 13.8 ms, was obtained in 14 h with a 2-s experiment repetition time. The principal values for the 13 single-bonded carbon chemical shift tensors are defined by the extracted powder patterns shown in Fig. 7b. Most notable are the significantly different powder patterns obtained for the lines at 28.1 and 28.5 ppm. Without TIGER processing it would have taken at least three times as long to obtain the PHORMAT 2D FID necessary to resolve the responses from these lines. The two sp^2 carbons in caryophyllene oxide whose isotropic shifts are 114.1 and 154.1 ppm have tensors with greater than 100-ppm span, which makes the extracted powder patterns difficult to interpret because of low S/N. The principal values of these two tensors were thus found from TIGER processing a second, specifically tailored PHORMAT dataset that

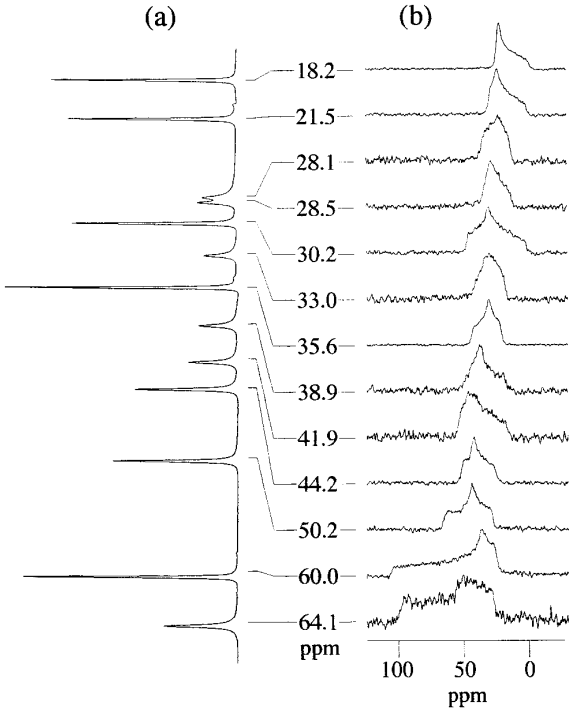

FIG. 7. Spectra obtained by TIGER processing a 2D ^{13}C PHORMAT spectrum of caryophyllene oxide. All data were taken with TPPM decoupling on a Chemagnetics CMX-400 spectrometer with a 7.5-mm diameter rotor, experiment repetition time = 2 s, cross-polarization contact time = 3 ms, γB_2 = 54.3 kHz, TPPM decoupler phase-shift angle = ±8.0°, and time at each phase = 9.2 μs, corresponding to a 180° pulse. All shifts shown are in parts per million from TMS, as found by referencing to adamantane at 38.4 ppm. (a) Portion of the high-speed MAS TOSS guide spectrum that includes the 13 lines from the single-bonded carbons. The spectrum is the Fourier transform of a 2500 complex point FID taken with sample spinning frequency = 4. kHz. The labels on the connecting lines give the isotropic shifts. (b) Extracted powder patterns for the 13 sp^3 carbons. The PHORMAT 2D FID was obtained with 220 complex points in the evolution dimension, evolution dwell time = 62.7 μs, 1024 complex points in the acquisition dimension, acquisition dwell time = 14.3 μs, and sample spinning frequency = 30.0 Hz.

took 4 h to acquire. Our work on caryophyllene oxide is still in progress, and thus the tensor principal values and the tensor assignments to specific carbons will be reported later.

Magic angle turning separated local field spectroscopy. The PHORMAT experiment can be extended to a third dimension (*19*) to encode dipolar coupling by including

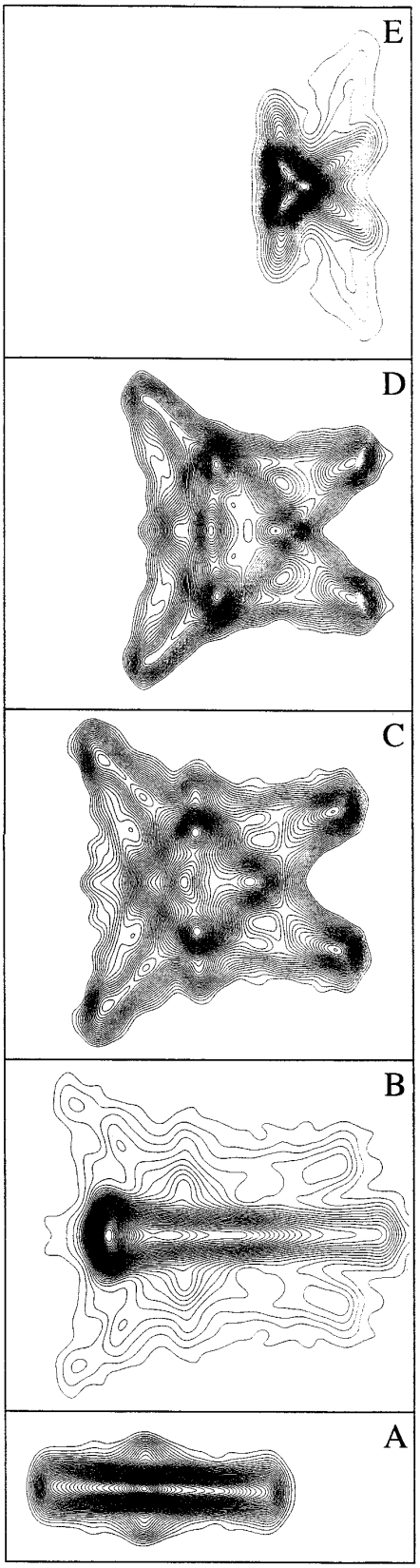

FIG. 8. Five 2D SLF spectra of 2,6-dimethoxynaphthalene extracted from a main FID with only 10 complex points in the isotropic-shift evolution dimension. The labels correspond to peak labels in Fig. 6. Chemical shift information is given on the horizontal axis, and dipolar information lies along the vertical axis.

a separated local field (SLF) (*20*) evolution period with flip-flop Lee-Goldburg homonuclear decoupling (*21*). The first evolution dimension with responses $g_{m,\rho}(t_b)$ remains the isotropic shift dimension, and it can be TIGER processed guided by a high-speed magic-angle-spinning FID. Such an experiment is defined by the noiseless 3D main FID

$$F_\rho(t_c, t_b, t_a) = \sum_{m=1}^{M} g_{m,\rho}(t_b) f_m(t_c, t_a), \qquad [15]$$

where t_c is a second evolution time. The estimates for the 2D FIDs are given by

$$\hat{f}_m(t_c, t_a) = \sum_{\rho=\text{real}}^{\text{imag}} \sum_{n=1}^{N} h_{m,\rho,n} E_\rho(t_c, \tau_n, t_a), \qquad [16]$$

where the $h_{m,\rho,n}$ are given as before by Eqs. [8] and [9]. The extracted 2D FIDs $\hat{f}_m(t_c, t_a)$ display the dipolar evolution dimension and the chemical shift powder pattern acquisition dimension. A separate spectrum is obtained for each isotropic shift. Figure 8 shows the five 2D SLF spectra of 2,6-dimethoxynaphthalene extracted from a main FID with only 10 complex points in the isotropic-shift evolution dimension. The distinct SLF patterns from the two carbons represented by peak B are visible; the nonprotonated carbon produces the narrow, intense band, while the protonated carbon produces the relatively low-lying characteristic SLF butterfly pattern. These spectra can be compared to those published previously (*19*) that were produced from a far more extensive dataset.

DISCUSSION

TIGER can also employ a multidimensional FID as its guide. Again, the only requirement is that the main FID model conform to the sum-of-products form. Thus one can imagine a 5D main FID on which models from a 2D guide FID are used to extract 3D FIDs. Such a 5D main FID is defined by the model

$$F(t_e, t_d, t_c, t_b, t_a) = \sum_{m=1}^{M} g_m(t_d, t_b) f_m(t_e, t_c, t_a). \qquad [17]$$

The 2D guide FID would define the responses in the t_b and t_d evolution dimensions, and a set of 3D FIDs with the t_c and t_d evolution dimensions and the t_a acquisition dimension would be extracted. An example of where such 2D-guide-FID TIGER processing could be useful is the 2D single-crystal chemical-shift-correlation experiment combined with separated local field spectroscopy to define a 3D experiment (*22*). The 2D chemical-shift-correlation data would be the guide FID, and a 1D separated-local-field spectrum would be extracted for each peak. The two- to threefold time savings afforded by TIGER processing would be especially useful in such high dimensionality cases.

Though the main FIDs of many spectroscopies, particularly those that produce narrow peaks, conform to the sum-of-products form necessary for the application of TIGER, this form is not universal. Two-dimensional powder patterns are notable exceptions.

Some variants of the MAT experiment produce tilted spectra that in their unprocessed states do not conform to the sum-of-products form (*1, 15*). Nevertheless, TIGER could treat such spectra by first transforming the acquisition dimension, applying an acquisition-dimension-frequency dependent shift to the evolution dimension FIDs, and then applying the TIGER algorithm to the modified evolution dimension to extract the powder pattern acquisition spectra.

TIGER is quite different from both linear prediction (*6*) and maximum entropy (*7*), both of which seek to increase resolution from the data in the main FID, rather than to import resolution from a separate guide FID. Linear prediction may be used profitably to analyze and decompose the 1D guide FID, a task that is currently done manually, making it the time-consuming step.

CONCLUSIONS

TIGER is a powerful method for combining the best features of two data sets, the resolution present in the guide FID and the correlation information available from the main FID. TIGER illustrates the principle that bringing outside knowledge into a data analysis can greatly enhance its accuracy and sensitivity.

ACKNOWLEDGMENTS

We thank Jim Harper for assistance in identifying caryophyllene oxide as an appropriate example molecule, and for providing the purified sample. This work was supported by the National Institutes of Health under Grant GM08521-36 from the Institute of General Medical Sciences, and by the Department of Energy under Contract DE-FG02-94ER14452 from the Division of Chemical Sciences of the Office of Basic Energy Sciences.

REFERENCES

1. Z. Gan, *J. Am. Chem. Soc.* **114,** 8307 (1992).
2. J. Z. Hu, W. Wang, F. Liu, M. S. Solum, D. W. Alderman, R. J. Pugmire, and D. M. Grant, *J. Magn. Reson. A* **113,** 210 (1994).
3. C. M. Carter, D. W. Alderman, and D. M. Grant, *J. Magn. Reson.* **73,** 114 (1987).
4. M. H. Sherwood, D. W. Alderman, and D. M. Grant, *J. Magn. Reson.* **84,** 466 (1989).
5a. Y. Manassen, G. Navon, and C. T. W. Moonen, *J. Magn. Reson.* **72,** 551 (1987).
5b. Y. Manassen and G. Navon, *J. Magn. Reson.* **79,** 291 (1988).

6. (a) R. Kumaresen and D. W. Tufts, *IEEE Trans.* **ASSP-30,** 833 (1982); (b) H. Barkhuijsen, R. De Beer, W. M. M. J. Bovee, and D. van Ormondt, *J. Magn. Reson.* **61,** 465 (1985); (c) H. Gesmar and J. J. Led, *J. Magn. Reson.* **83,** 53 (1989).
7. J. A. Jones and P. J. Hore, *J. Magn. Reson.* **92,** 363 (1991).
8. R. J. Iuliucci and D. M. Grant, *Solid State NMR* **6,** 55 (1996).
9. R. R. Ernst, G. Bodenhausen, and A. Wokaun, ''Principles of Nuclear Magnetic Resonance in One and Two Dimensions,'' pp. 301–308, Oxford Univ. Press, Oxford, 1991.
10. D. J. States, R. A. Haberkorn, and D. J. Ruben, *J. Magn. Reson.* **48,** 286 (1982).
11. W. C. Hamilton, ''Statistics in Physical Science,'' Ronald Press, New York, 1964.
12. F. A. Graybill, ''Theory and Application of the Linear Model,'' Wadsworth and Brooks/Cole, Pacific Grove, 1976.
13. F. Liu, C. G. Phung, D. W. Alderman, and D. M. Grant, *J. Magn. Reson. A* **120,** 231 (1996).
14. F. Liu, C. G. Phung, D. W. Alderman, and D. M. Grant, *J. Am. Chem. Soc.* **118,** 10629 (1996).
15. Z. Gan and R. R. Ernst, *J. Magn. Reson. A* **123,** 140 (1996).
16. (a) W. T. Dixon, *J. Chem. Phys.* **77,** 1800 (1982); (b) W. T. Dixon, J. Schaefer, M. D. Seficik, E. O. Stejskal, and K. A. McKay, *J. Magn. Reson.* **49,** 341 (1982).
17. D. W. Alderman, M. S. Solum, and D. M. Grant, *J. Chem. Phys.* **84,** 3717 (1986).
18. A. E. Bennett, C. M. Rienstra, M. Auger, K. V. Lakshmi, and R. G. Griffin, *J. Chem. Phys.* **103,** 6951 (1995).
19. J. Z. Hu, D. W. Alderman, R. J. Pugmire, and D. M. Grant, *J. Magn. Reson.* **126,** 120 (1997).
20. R. K. Hester, J. L. Ackerman, B. L. Neff, and J. S. Waugh, *Phys. Rev. Lett.* **36,** 1081 (1976).
21. M. Lee and W. I. Goldburg, *Phys. Rev. A* **140,** 1261 (1965).
22. M. H. Sherwood, D. W. Alderman, and D. M. Grant, *J. Magn. Reson. A* **104,** 132 (1993).